Inorganic Chemistry Communications 171 (2025) 113521

Contents lists available at ScienceDirect

Inorganic Chemistry Communications

journal homepage: www.elsevier.com/locate/inoche

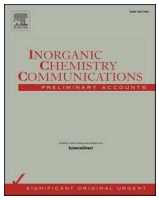

Short communication

Anticancer evaluation of Co(III) complex derived from 1-isonicotinoyl-4-(4-nitrophenyl)-3-thiosemicarbazide: Structural characterization, photophysical, and Hirshfeld studies

Ram Nayan Gautam [a], Alok Shukla [b], Suryansh Chandra [a], Sundeep Kumar [c], A. Acharya [b], Mamata Singh [d], R.J. Butcher [e], M.K. Bharty [a,*]

[a] Department of Chemistry, Banaras Hindu University, Varanasi 221005, India
[b] Department of Zoology, Banaras Hindu University, Varanasi 221005, India
[c] Department of Applied Chemistry, F.E.T, M.J.P. Rohilkhand University, Bareilly 243006, India
[d] Infectious Disease Division, Mayo Clinic, Jacksonville, FL, USA
[e] Department of Chemistry, Howard University, 525 College Street NW, Washington, DC 20059, USA

ARTICLE INFO

Keywords:
Crystal structure
Co(III) complex
Anticancer
Human glioblastoma
Hirshfeld surface analysis

ABSTRACT

A new cationic complex, [Co((*intph*)(*en*)$_2$]Cl, derived from the 1-isonicotinoyl-4-(4-nitrophenyl)-3-thiosemicarbazide (H_2*intph*), is reported. The synthesized ligand and its corresponding Co(III) complex were successfully characterized by applying FT-IR and UV–visible spectroscopic techniques and single crystal ray diffraction data. Molecular geometries of the ligand and its Co(III) complex were accurately determined from their respective X-ray crystallographic analysis. The ligand and [Co((*intph*)(*en*)$_2$]Cl crystallize in Triclinic *and* monoclinic systems with space groups P-1 and P $2_1/n$, respectively. The crystal structures of H_2*intph* and [Co((*intph*)(*en*)$_2$]Cl are stabilized by weak C-H···O, N-H···O, and C-H···Cl hydrogen bonding interactions. Hirshfeld surface analysis was accomplished to investigate intermolecular hydrogen bonding interactions found in ligand H_2intph and [Co((intph)(en)$_2$]Cl. The cytotoxicity of the ligand and the complex [Co((intph)(en)$_2$]Cl was assessed for their anticancer potential against human glioblastoma (U87) and Dalton lymphoma (DL) cell lines. The complex exhibited IC_{50} values of 100 μg/mL for U87 cells and 120 μg/mL for DL cells, indicating the concentration at which 50 % of cell viability was inhibited. In comparison, the ligand was less effective in the MTT assay against both U87 and DL cells. These results suggest that the complex [Co((intph)(en)$_2$]Cl significantly reduces glioblastoma cell viability. Treatment with the complex induced cell death through both apoptotic and necrotic pathways, as evidenced by Hoechst/PI double staining. Additionally, there was an increase in intracellular reactive oxygen species (ROS), highlighting the role of oxidative stress in the anticancer activity of the [Co((intph)(en)$_2$]Cl complex. Furthermore, fluorescence studies were carried out which revealed the order of fluorescence behaviors between the ligand and the Co(III) complex to be Co(III) complex > H_2*intph*.

1. Introduction

Glioblastoma is a highly aggressive and heterogeneous brain cancer that is resistant to the many traditional treatments involving surgery or radiation [1–3]. Its infiltrative nature makes the complete removal of tumor cells challenging, leading to a poor prognosis for glioma patients [4]. Various resistance mechanisms prevent the progress made in the therapy of this kind of brain tumor. Furthermore, glioblastoma's extreme heterogeneity promotes escape mechanisms from targeted therapies and hinders a drug's ability to effectively manage the entire tumor mass, both of which are major contributors to treatment resistance [5]. The discovery of several metal complexes in recent years, such as carboplatin and cisplatin, has greatly impacted contemporary cancer therapies. This drug exhibits certain side including nausea, nephrotoxicity, Cardiotoxicity, hepatotoxicity, and neurotoxicity [6]. Over the last three decades, extensive research has focused on exploring the anticancer potential of cobalt complexes. Significant efforts have been made to comprehend the mechanisms by which these complexes exert their antiproliferative effects [7–9]. This viewpoint provides a detailed analysis of the mechanisms, and so highlights the developments in

* Corresponding author.
E-mail address: mkbharty@bhu.ac.in (M.K. Bharty).

https://doi.org/10.1016/j.inoche.2024.113521
Received 17 August 2024; Received in revised form 24 October 2024; Accepted 5 November 2024
Available online 15 November 2024

antiproliferative cobalt complexes. Moreover, several cobalt complexes have been reported to exhibit potent anticancer properties, making them a subject of considerable interest in the field of cancer research [10]. Cobalt metal is a relevant element in living system, and it has been observed that several enzymes depend on it to function [11,12]. Further, cobalt metal plays a prominent role in sustaining life and exists naturally as vitamin B_{12}, which is considered to be an essential molecule for the normal growth of red blood cells and the normal functioning of the brain and nerves [13]. Thus, it may reasonably be speculated that cobalt and cobalt-based complexes would have less side effects as compared to platinum complexes. The thiosemicarbazides have been used to be a versatile ligand due to their unique chelating ability which assists them to bond with various metals *via* several bonding modes, and their chemical, biological, and antitumor activities as well [14–19]. Regarding the biological effects, thiosemicarbazide complexes demonstrate anticancer and therapeutic effects because they can permeate through the semipermeable membrane of the cells [20]. The increased lipophilicity character of the metal complexes in comparison to the free ligand may be the cause of the heightened impact [21,22]. The heightened impact of these types of complexes as compared to the free ligands can be due to their enhanced membrane permeability, boosted stability, ability to target hydrophobic binding sites, and effective cellular uptake mechanisms which cooperatively contribute to the increased effectiveness and biological activity of lipophilic metal complexes [23–29]. While numerous papers have been reported on the metal complexes of substituted thiosemicarbazide [30–33], limited information is currently available on the anticancer activity of mixed ligand complexes incorporating nitrogen sulfur-containing ligands alongside *o*-phen, 2,2′-bipyridyl, or ethylenediamine as auxiliary ligands. Because of the above interest, we report the synthesis, spectral, photoluminescence, and structural, characterizations of Co(III) complex of 1-isonicotinoyl-4-(4-nitrophenyl)-3-thiosemicarbazide (H_2*intph*). We have investigated the tumoricidal activities of ligand H_2*intph* and its Co(III) complex against the *glioblastoma cell line* (U87). The results indicate that ligand H_2*intph* and its Co(III) complex have significant tumoricidal activity against U87 cells concerning cell death *via* both apoptotic and necrotic modes as revealed by Hoechst/PI double staining and generation of the intracellular ROS. The Co(III) complex showed a competitive tumoricidal effect as compared to the free ligand.

2. Experimental

2.1. Synthesis of 1-isonicotinic-4-(4-nitrophenyl)-3-thiosemicarbazide (H_2*intph*)

The compound 1-isonicotinoyl-4-(4-nitrophenyl)-3-thiosemicarbazide was produced after the refluxing of isonicotinic hydrazide (2.74 g, 20 mmol) with 4-nitrophenyl isothiocyanate (3.60 g, 20 mmol) using an equimolar ratio (1:1) for a duration of 6 h. After the completion of this reaction, an orange precipitate was obtained, which was subsequently filtered and washed many times using a 50 % (v/v) mixture of water and ether. Yield: 79 %, m.p. 209–211 °C, Anal. found (%): C, 49.40; H, 3.55; N, 21.90; S, 10.25 for $C_{13}H_{12}N_5O_3S$ (317.33) Calcd (%): C, 49.05; H, 3.80; N, 22.00; S, 10.07. IR data (ν cm^{-1}, KBr): 3436 ν(OH), 3273, 3100 ν(NH); 1620 ν(C═O); 1556, 1316 $\nu(NO_2)$, 1058 ν(N–N), 952 ν(C═S). UV–vis (λ_{max}, DMSO, nm) 348. NMR data ^{1}H NMR (600 MHz, DMSOd_6 (δ, ppm): 11.02 (s, 1H), 10.29 (s, 1H), 10.20 (s, 1H), 8.84 (d, J = 6.2 Hz, 2H), 8.28 – 8.25 (m, 2H), 7.92–7.90 (m, 4H). ^{13}C NMR (151 MHz, DMSOd_6 (δ, ppm) δ 181.20, 165.00, 150.77, 146.04, 144.06, 139.82, 125.49, 124.11, 122.13. The single crystal x-ray data shows that the nitro group of the ligand (H_2intph) along with the benzene ring is disordered.

2.2. Synthesis of [Co(intph)(en)$_2$]Cl

A methanolic solution of $CoCl_2{\cdot}6H_2O$ (1 mmol,0.238 g) was mixed with a solution of H_2*intph* (2 mmol, 0.634 g) in MeOH/$CHCl_3$ (10 mL). The reaction mixture was then stirred for 4 hrs at ambient temperature which yielded a greenish precipitate. Subsequently, ethylenediamine (0.156 g, 1 mmol) was slowly mixed with constant stirring for 1 h, which dissolved the precipitate to produce the homogenous solution. The solution so obtained was stored undisturbed for crystal growth. Mountable green crystals of the desired Co(III) complex, suitable for X-ray analysis, were expectedly developed after the gradual evaporation of the solvent over a period of 15 days. **Yield:** 62 %, Decomposition temperature >235 °C, Anal. found (%): C, 38.30; H, 4.90; N, 23.55; S, 6.15 for $C_{17}H_{25}ClCoN_9O_3S$ (529.90) Calcd (%): C, 38.53; H, 4.76; N, 23.79; S, 6.05. IR data (ν cm^{-1}, KBr): 3289, 3164, ν(NH); 1642 ν(C═O); 1567, 1328 $\nu(NO_2)$, 1113 ν(N–N), 848 ν(C–S), 584 ν(M–N), 502 ν(M–S). UV–vis (λ_{max}, DMSO, nm) 362 and 504 nm. NMR data ^{1}H NMR (600 MHz, DMSOd_6 (δ, ppm): 9.50 (s, 1H), 3.43 (NH_2), and 2.09 (CH_2), 8.84 (d), 8.01 – 8.61 (m, 4H), 7.11–7.26 (m, 4H). ^{13}C NMR (151 MHz, DMSOd_6 (δ, ppm) δ 206.49, 161.84, 150.79, 149.15, 152.40, 121.09, 119.19, 117.82, 115.74, 30.65.

3. Results and discussion

The wide spectrum of cancers effectively treated by platinum-based agents, such as *cisplatin* and *carboplatin*, has subsequently prompted extensive research on the development of alternative transition metal-based compounds with promising cytostatic properties [9]. Resistance and side effects associated with platinum drugs have underscored the need for novel therapies. Cobalt complexes, recognized for their potential anticancer activity, have emerged as promising candidates [34,10]. In this study, the anticancer effects of a cobalt(III) complex of thiosemicarbazide have been investigated against human *glioblastoma cells*. A significant dose-dependent reduction in cell viability of U87 cells has been observed being indicative of the potent anticancer activity of the complex [Co(*intph*)(en)$_2$]Cl. Our results demonstrate a significant increase in the intracelllular ROS levels upon treatment which suggests that the enhanced intracellular oxidative stress is responsible for the observed cytotoxicity. The grinish crystalline [Co(*intph*)(en)$_2$]Cl complex was obtained after stirring a methanolic solution of a hydrated Co (II) salt and H_2*intph* ligand (derived after refluxing isonicotinic hydrazide with 4-nitrophenyl isothiocyanate in an equimolar ratio (1:1)) in the presence of ethylenediamine at room temperature as illustrated in Scheme 1. The H_2*intph* ligand and its [Co(*intph*)(en)$_2$]Cl complex were found to be crystalline solids, stable, and air/moisture resistant at room temperature, and were structurally characterized by employing various spectroscopic techniques (UV–vis, FT-IR and ^{1}H & ^{13}C NMR). Subsequently, orange and green crystals of H_2*intph* ligand and its Co(III) complex, suitable for single crystal X-ray crystallography (block-shaped

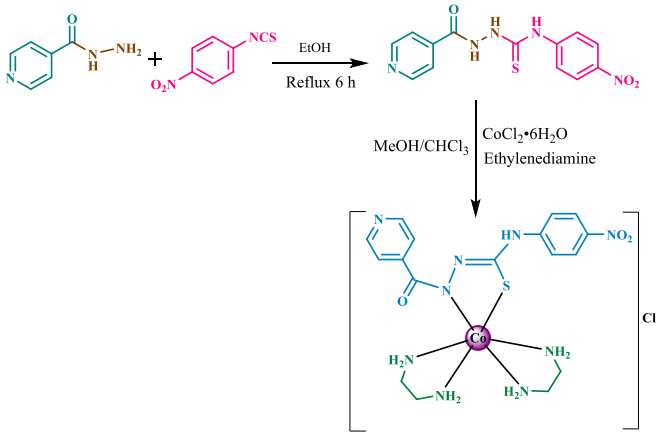

Scheme 1. Schematic routes for the synthesis of H_2intph and its [Co(*intph*)(en)$_2$]Cl complex.

(0.305 × 0.301 × 0.123 mm^3) and plate-shaped (0.303 × 0.214 × 0.125 mm^3), respectively), were grown after the gradual evaporation of solvent at room temperature over a period of time. It is evident from the X-ray crystallographic analysis of the [Co(*intph*)(en)$_2$]Cl complex that it gets crystallized in a monoclinic crystal system with a P21/n space group, and exhibits an irregular distorted octahedral geometry. The complex is seen to behave as cationic in nature, and the charge over the coordination sphere is satisfied by the univalent Cl^- counter ion. Apparently, the central Co(III) metal ion is surrounded equatorially by the three N and one S donor atoms of the bidentate **H$_2$*intph*** ligand and the symmetrical ethylene diamine (en) co-ligand units, whereas the axial coordination sites are occupied by the two N donor atoms of the co-ligand units rendering a significant deviation from an ideal octahedral geometry.

3.1. Crystal structure description

The molecular strucutres of H$_2$*intph* ligand and [Co(*intph*)(en)$_2$]Cl complex were ascertained by single crystal X-ray diffraction analysis. Crystallographic data and structure refinement parameters, pertaining to H$_2$*intph* ligand and [Co(*intph*)(en)$_2$]Cl complex, are included in Table 1. The relevant interatomic parameters of H$_2$*intph* ligand and [Co(*intph*)(en)$_2$]Cl are selected, and subsequently compiled in the Supplementary Tables 1 and 3 respectively. Hydrogen bond parameters for ligand and complex are given in Supplementary Tables 2 and 4.

3.1.1. Crystal description of H_2intph ligand

The bidentate dibasic ligand, H$_2$*intph* was carefully analysed by single crystal X-ray diffraction crystallography in order to ascertain the plausible molecular structure and conformation of the prevailing tautomeric isomer in the crystalline phase. The molecular structure along with schematic labelled atoms of the H$_2$*intph* ligand is illustrated in Fig. 3. Apparently, the H$_2$*intph* ligand is crystallized in a triclinic crystal system with a P-1 space group containing two independent molecules in the asymmetric unit. The structure contains a cation and an anion pair in the H$_2$*intph* moiety. The cation is the protonated pyridine ring (N1a) and the anion is the molecule where the OH proton has been lost. This enables the two molecules to form planar sheets with strong hydrogen bonding as shown in Supplementary Fig. 7. The nitrophenyl ring and nitro groups are disordered in the compound. A thorough inspection of the crystal structure reveals that the H$_2$intph molecule prefers to exist in the N4a-amino/N3a-amino/N2a-imine/S1a-thione/O1a-enol tautomeric form in the crystalline phase as is indicated by the presence of the amino hydrogens near the N4a and N3a atoms and absence of hydrogen around N2a atom which shifted to pyridine nitrogen N1a (Supplementary Fig. 7). The prevailing tautomeric form of the ligand is further supported by the S1a-C7a = 1.6683(15) bond length which was observed to be consistent with that reported earlier for the thione group [35,36]. The N2a-C6a = 1.2871(18) bond length is measured to be comparatively shorter as compared to N3a-C7a = 1.3541 (19) bond length which clearly implies a double bond character in the N2a-C6a bond. The O1a-C6a = 1.3004(17) bond length is found to be significantly longer than that is mentioned earlier for the carbonyl group, C═O = 1.213(3) and 1.239 Å [37,38] which rules out any possibility of the carbonyl moiety in the existing tautomeric form of the ligand. The ligand is seen to exhibit *trans–cis-trans–trans* conformation as is evident from the torsion angles C8a-N4a-C7a-N3a; N4a-C7a-N3a-N2a; C7a-N3a-N2a-C6a and N3a-N2a-C6a-C1a which were measured to be 175.78(16), −5.0(2), −177.42(15) and 178.11(13), respectively. Further, the S1a = C7a group appears to be aligned *trans* and *cis* with respect to N2a-N3a and N4a–C8a bonds in the same way as described in the crystal structure of similar thiosemicarbazide ligand and can be attributed to the torsion angles S1a-C7a-N3a-N2a and S1a-C7a-N4a-C8a of 175.47 (12) and −4.7(3), respectively [35]. Moreover, the –NO_2 group and benzene ring exhibit a significant thermal disorder and are observed to be almost coplanar with each other in the molecule as indicated by the O2a-N5a-C11a-C12a = -173.6 (4), O3a-N5a-C11a-C12a = 8.0 (5). The crystal structure of the H$_2$*intph* is stabilized by N-H···O weak interactions found among the thioamide NH and carbonyl oxygen. Further, the structure is also stabilized by the O-H···O interactions occurring amongst the enolic OH of a cationic unit of the ligand and carbonyl oxygen of another anionic unit of the ligand moiety leading planar architectures (Supplementary Fig. 7).

Table 1
Crystallographic data and structure refinement parameters for H$_2$*intph* and [Co(*intph*)(en)$_2$]Cl.

	Ligand	Complex
Empirical formula	$C_{26}H_{22}N_{10}O_6S_2$	$C_{17}H_{25}ClCoN_9O_3S$
Formula weight	634.65	529.90
Crystal system	*Triclinic*	*Monoclinic*
Space group	$P\bar{1}$	$P\,2_1/n$
T (K)	293(2) K	293(2) K
λ, Cu/Mo k_α (Å)	1.54184	0.71073
Unit cell dimensions		
a (Å)	7.8095(2)	7.4960(3)
b (Å)	13.4092(3)	15.6447(6)
c (Å)	14.1157(2)	19.0036(6)
α (°)	98.9270(10)	90
β (°)	100.4110(10).	91.241(3)
γ (°)	93.021(2)	90
V(Å^3)	1431.27(5)	2228.08(14)
Z	2	4
$\rho_{calc.}$ (g cm^{-3})	1.473	1.580
μ (mm^{-1})	2.214	1.024
F(000)	656	1096
Crystal size (mm)	0.45 × 0.41 × 0.12	0.28 × 0.24 × 0.18
θ range for data collection (°)	3.229 to 78.671	2.503 to 26.927
Index ranges	− 9≤ h ≤ 9, − 16≤ k ≤ 17 − 17≤ l ≤ 11	− 9≤ h ≤ 9, − 14≤ k ≤ 19 − 24≤ l ≤ 23
Number of reflections collected	17,238	16,677
Number of independent reflections (R_{int})	5861(0.0225)	4584 (0.0489)
Data/restraints/parameters	5861/162/474	4584/0/289
Goodness-of-fit (GooF) on F^2	1.082	1.061
R_1[a] wR_2^b [I > 2σ(I)]	0.0418, 0.1220	0.0508, 0.1039
R_1[a] wR_2^b (all data)	0.0477, 0.1283	0.0808, 0.1175
Largest difference in peak/hole (e. Å^{-3})	0.309, −0.348	0.463, −0.367

[a] $R_1 = \Sigma||F_o| - |Fc||/\Sigma|F_o|$. [b] $R_2 = [\Sigma w(|F_o^2| - |F_c^2|)^2/\Sigma w|F_o^2|^2]^{1/2}$.

3.1.2. Crystal description of [Co(intph)(en)$_2$]Cl complex

The X-ray crystallographic analysis of [Co(*intph*)(en)$_2$]Cl complex reveals it to be crystallized in a monoclinic crystal system with a P 21/n space group, and adopted an irregular distorted octahedral geometry around the Co(III) ion as depicted in Fig. 4. In the complex, bidentate dibasic H$_2$*intph* ligand is coordinated to the central Co(III) metal ion through its thione S and imine N atoms, and the other coordination sites are occupied by the four N donor atoms of the two symmetrical ethylene diamine (en) co-ligand units. It is evident that the Co(III) complex preferably exists as cationic in nature, and the positive charge over the coordination sphere is compensated by the negative chloride counterion. The bite angles, N(2)–Co-S(1), N(6)–Co-N(7) and N(9)–Co-N(8), in the five-membered chelate rings around the central Co(III) metal ion, were measured to be 84.41, 84.91, and 85.43°, respectively, which indicates a significant deviation from an ideal octahedral geometry [25,39–42]. Apparently, the bond length between the central Co(III) metal ion and N2 donor atom of the ligand moiety (Co–N2 = 1.946 (2)) was observed to be relatively short as compared to the other Co–N bond lengths (Co–N6 = 1.951(3), Co–N9 = 1.966(3), Co–N8 = 1.968(2) and Co–N7 = 1.978(2)) which substantiates a strong bonding interaction between the N donor atom of the ligand moiety and the central Co(III) metal ion than the ethylene diamine nitrogen atoms [43,44]. Moreover, the five-membered chelate ring and the pyridine ring of the coordinated ligand did not appear to be perpendicular as evidenced by the dihedral

angle that was measured to be 53.79° between the two rings. The structure of the Co(*intph*)(en)$_2$]Cl is substantial by C-H···O and N-H···O hydrogen bonding interactions between the CH and NH hydrogen of the ligand moiety and carbonyl oxygen atom of the nearby unit of the ligand. Further, the structure is also stabilized by N-H···N hydrogen bonding interactions found between NH hydrogen atoms of ethylene diamine molecule and pyridine N atoms of another nearby moiety of the ligand leading to a butter-like architecture in the complex. (Supplementary Fig. 8). In addition, C-H···Cl and N-H···Cl interactions stabilize the structure of the complex found between CH hydrogen of phenyl ring/ thioamide NH hydrogen of ligand moiety and chloride atom present outside the coordination sphere leading to a linear chain structure (Supplementary Fig. 9).

3.2. IR spectra

The IR spectrum of ligand 1-isonicotinic-4-(4-nitrophenyl)-3-thiosemicarbazide (H$_2$*intph*) shows a broad band at 3436 cm^{-1} suggesting that the OH group present in the H$_2$*intph* molecule. Two absorptions were observed at 3273 and 3100 cm^{-1} owing to the N–H stretching vibration of the amide and thioamide group. In addition, two more bands were observed at 1620 and 1024 cm^{-1} due to carbonyl group (C═O) and N-N stretching vibrations, respectively (Supplementary Fig. 1). There is a slightly negative shift observed in the ν(C═O) group of the ligand than the other reported thiosemicarbazide ligand suggesting that the ν(C═O) is converted to OH form which is further supported by the OH group absorption band which is also confirmed by X-Ray data. A band appeared at 952 cm^{-1} due to ν(C═S) stretching vibration. Two more absorption bands were observed at 1556 and 1337 cm^{-1} due to the asymmetrical and symmetrical NO_2 stretching vibrations. The IR spectrum of the Co(III) complex shows a band at 3164 cm^{-1} due to the NH group attached to the phenyl ring, however, one more NH band appeared at 3289 cm^{-1} owing to NH_2 stretching vibrations of the ethylenediamine molecules. Thus, IR data suggest that after complexation, two NH protons were lost and coordinated through Co(III) ion generating a five-membered chelate ring (Supplementary Fig. 2). The positive shifts of about 22 cm^{-1} in the ν(C═O) band indicate the electron density of the C═O group slightly shifted onto nitrogen atoms and the carbonyl group was not involved in coordination. One new band was observed at 1587 cm^{-1}, which confirmed the conversion of the carbon–nitrogen (C-N) single bond to the carbon–nitrogen (C═N) bond due to the enolization of NH proton to SH proton [45]. Two more absorption bands were observed at 1567 and 1328 cm^{-1} due to the asymmetrical and symmetrical NO_2 stretching vibrations. Complex shows additional bands for (Co-N) and (Co-S) at 584 and 502 cm^{-1} signifying the coordinating of Co (III) with one hydrazine nitrogen and thiol sulfur, respectively. Thus, the Infra-red spectral data of the Co(III) complex suggest that ligand H$_2$*intph* acts as a di-negative bidentate.

3.3. ^{1}H and ^{13}C NMR spectra

The ^{1}H NMR spectrum of H$_2$intph exhibits three signals at δ 11.02, 10.29, and 10.20 ppm, corresponding to the amide and thioamide NH protons, respectively. The aromatic proton of the isoniazid pyridine ring displays signals in the range of 8.84–8.25 ppm, while the nitrophenyl ring protons appear in the range of 7.92–7.90 ppm (Supplementary Fig. 3). ^{13}C NMR spectrum of H$_2$intph shows two signals at 181.20 and 165.00 ppm due to C═S carbon and C═O carbons, respectively. All the aromatic ring carbons appear in the range of 122.13 – 150.77 ppm (Supplementary Fig. 4). The ^{1}H NMR spectrum of diamagnetic complex [Co(intph)(en)$_2$]Cl exhibits the loss of two NH protons (amide and thioamide) and appeared only one signal at δ 9.50, ppm, due to NH proton near the phenyl ring of the ligand moiety which indicates that both NH protons involved in bonding with Co(III) ion. Two other signals were also observed at 3.43, and 2.09 ppm owing to the NH_2 and CH_2 protons of ethylenediamine molecules. The isoniazid pyridine ring protons appear in the range of 8.01–8.61 ppm, whereas the nitrophenyl ring protons appear in the range of 7.11–7.26 ppm (Supplementary Fig. 5). ^{13}C NMR spectrum of [Co(intph)(en)$_2$]Cl shows two signals at 206.49 and 161.84 due to C═S carbon and C═O carbons, respectively. All the aromatic ring carbons appear in the range of 115.74–150.79 ppm (Supplementary Fig. 6). In addition, one more signal was observed at 30.65 ppm due to the CH_2 protons of the ethylenediamine protons.

3.4. Electronic spectra

The UV–vis spectra of both ligand (H$_2$*intph*) and [Co(*intph*)(en)$_2$]Cl complex as shown in Fig. 1, display two distinct absorption bands at 348 and 362 nm, respectively which may be attributed to π-π*/intra ligand electronic transitions. The absorption band observed in the free ligand at 348 nm is shifted to the longer wavelength at 362 nm in the coordinated ligand which evidently supports the coordination of the ligand to the central Co(III) metal in the complex. [Co(*intph*)(en)$_2$]Cl is diamagnetic, and its electronic spectrum suggests the presence of Co(III) in a low-spin octahedral geometry. It shows a broad band at 504 nm, assigned to the $^1A_{1g} \rightarrow {}^1T_{1g}$ transition in the octahedral geometry around the Co(III) ion [46].

3.5. Photoluminescence studies

The emission spectra of ligand H$_2$*intph* and Co(III) complex (shown in Fig. 2) were obtained in a 10^{-5} M DMSO solution. H$_2$intph is found to exhibit a photoluminescent emission band located at 433 nm when excited at 348 nm. Nevertheless, upon excitation at 362 nm (27624 cm-1), [Co(intph)(en)$_2$]Cl exhibits an emission band at 446 nm (22421 cm^{-1}). Thus, the photoluminescence results confirm the fluorescence nature of both ligand H$_2$*intph* and its Co(III) complex, with an order being complex > H$_2$intp.

3.6. Hirshfeld surface analysis

Hirshfeld surface analysis was carried out to determine the quantitative nature of interactions existing in the ligand H$_2$intph and its complex [Co(*intph*)(en)$_2$]Cl. Using the standard Tonto code, Hirshfeld surfaces (HS) for H$_2$intph and complex [Co(intph)(en)$_2$]Cl were generated, revealing intermolecular hydrogen bonding interactions. Fig. 5 demonstrates the HS mapped over d_{norm}. The color conversion from red to blue to white varies depending on the contact distances associated

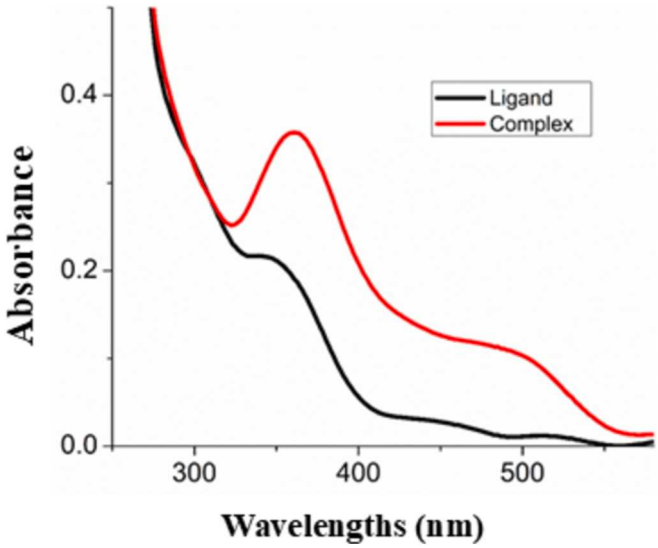

Fig. 1. UV–vis. absorption spectra of H$_2$intph and [Co(intph)(en)$_2$]Cl in 10^{-5} M DMSO.

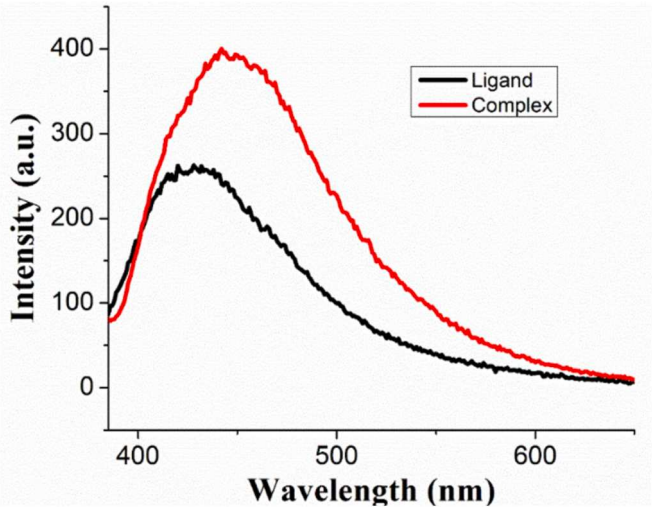

Fig. 2. Fluorescence spectra of H_2*intph* and [Co(*intph*)$(en)_2$]Cl obtained in 10^{-5} M DMSO.

with the sum of van der Waals radii, resulting in changes in the normalized contact distance, or d norm. The red, white, and blue sections of the dnorm surface, respectively signify close proximity, moderate proximity, and minimal proximity to the surrounding atoms [47–49]. The d_{norm} of ligand and complex show few dark red spots suggesting close proximity and stronger interaction with outside atoms (Fig. 5a-b).

Quantitative analysis of the intermolecular interactions present in both the ligand and Co(III) complex was achieved by summarizing their nature and type using 2-D fingerprint plots. These plots were generated by determining the 3-D dnorm surfaces of the H_2intph and [Co(*intph*)$(en)_2$]Cl. The impact of specific contacts and their respective regions on the norm was also scrutinized and compiled in Supplementary Figs. 10 and 11. One of the potential key supramolecular topologies identified is the H···H interaction. The H···H interaction, present in both the ligand and the complex, accounts for 23.0 % and 40.6 % of the interactions, respectively, making it the most dominant. Then, in ligand ***H_2intph*** and [Co(*intph*)$(en)_2$]Cl, O···H/H···O (total 25.1 % and 18.0 %, respectively) is another important interaction followed by C···H/H···C (total 13.7 % and 12.1 %, respectively)). Moreover, analysis reveals that both H_2intph and [Co(intph)$(en)_2$]Cl have 10.9 and 3.7 % of S···H/H···S interactions, respectively. Further, N···H/H···N interactions were found at 4.9 and 7.4 %, respectively in ligand and complex (Fig. 5c).

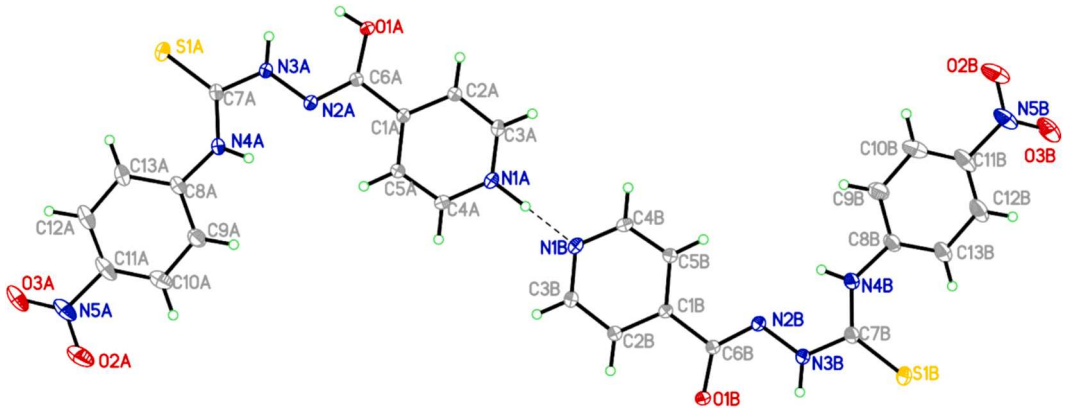

Fig. 3. ORTEP diagram of H_2intph (cation–anion pair form) with schematic labelled atoms.

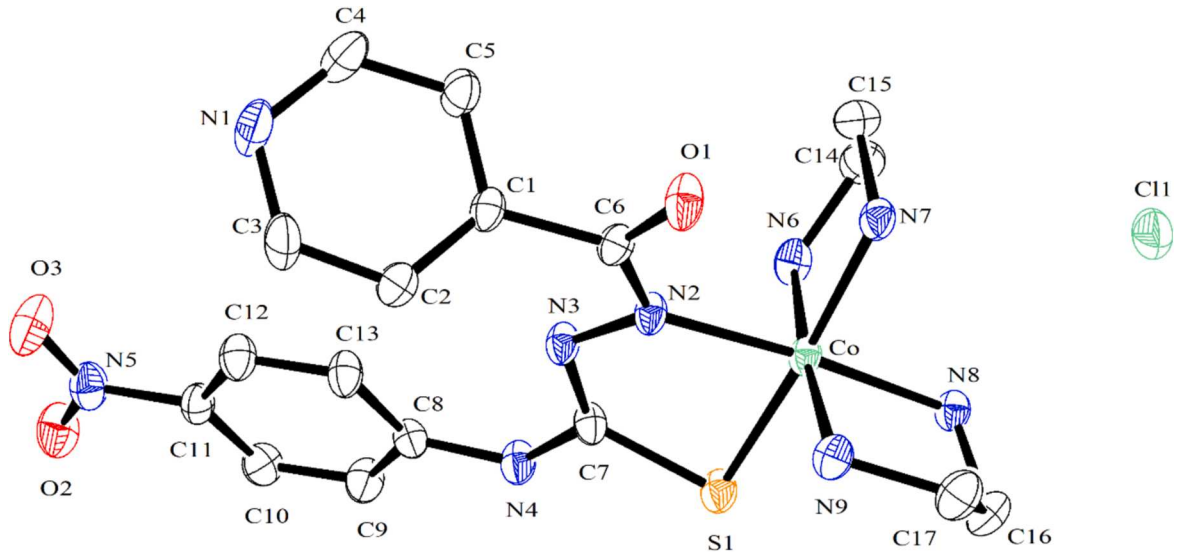

Fig. 4. ORTEP diagram of [Co(*intph*)$(en)_2$]Cl complex with schematic labelled atoms, drawn at 30 % thermal ellipsoid probability level excluding H atoms for clarity.

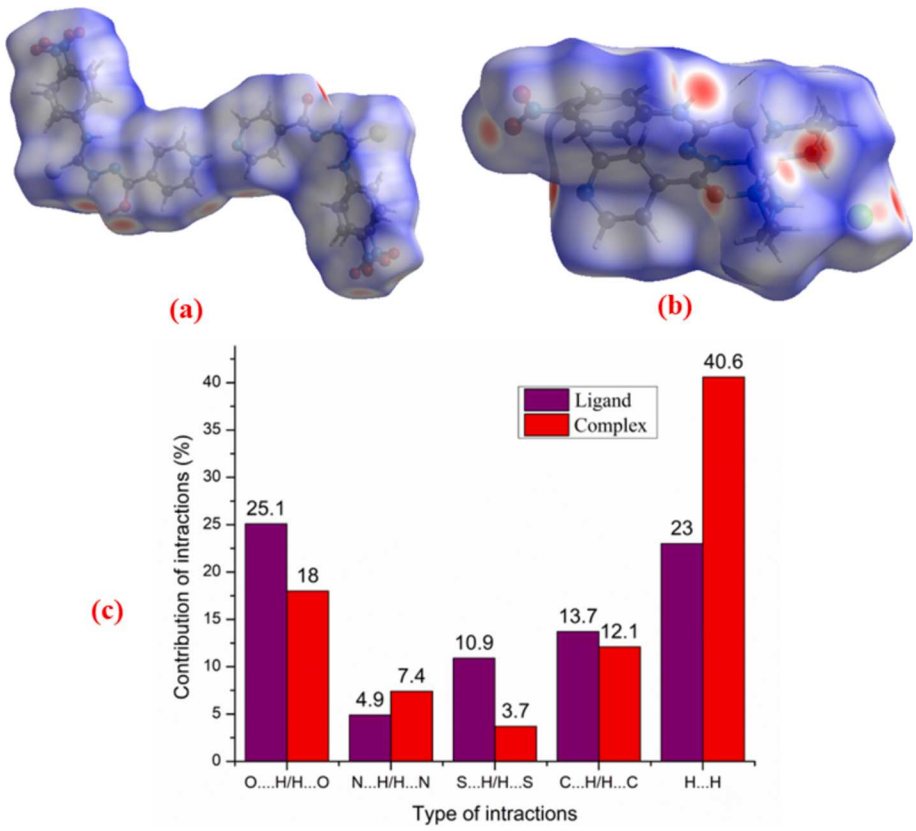

Fig. 5. (a) and (b) represent the HS of ligand and Co(II) complex mapped over d_{norm} and (c) Total contribution of individual interactions in ligand and complex.

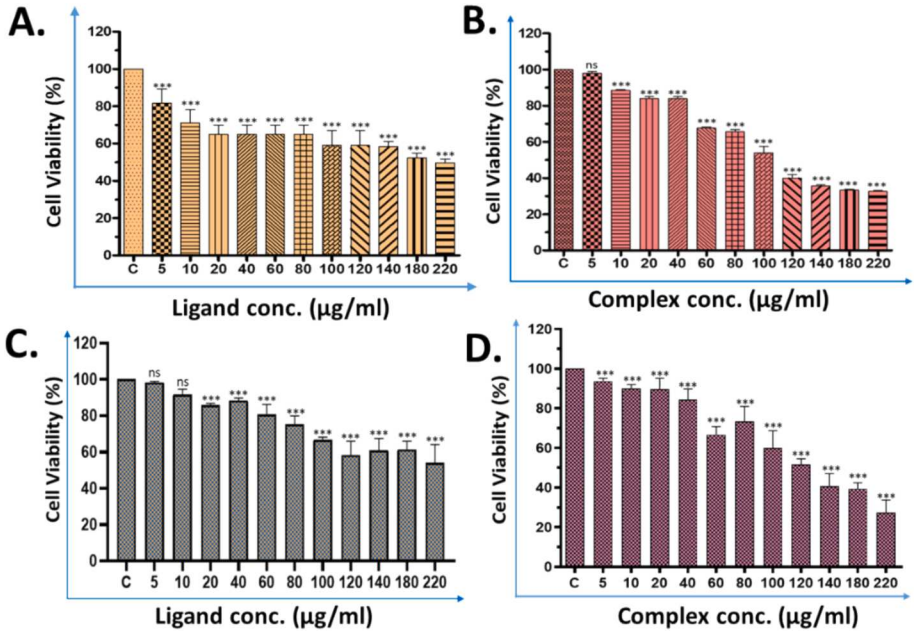

Fig. 6. Demonstrates the evaluation of cell viability using the standard MTT assay. (A) U-87 cells were exposed to the ligand at various concentrations for 24 h. (B) U-87 cells were exposed to the complex at various concentrations for 24 h. (C) DL cells were exposed to the ligand at various concentrations for 24 h. (D) DL cells were exposed to the complex at various concentrations for 24 h. The bar graph depicts the percentage of cell viability of both the Ligand and the complex on U-87 and DL cells respectively. Data were represented as a percentage of mean ± SD. Statistical analysis involved a one-way analysis of variance, followed by a post hoc Dunnett's Multiple Comparison test, conducted across a minimum of three independent experiments. Significance level was measured at ***$p < 0.001$.

3.7. Anticancer activity

3.7.1. [Co(intph)(en)$_2$]Cl treatment reduced cell viability of U87 cells and DL cells

Our results indicated that the complex [Co(intph)(en)$_2$]Cl exhibited greater potency in inhibiting U87 cell viability compared to the ligand (Fig. 6A and B). Specifically, the [Co(intph)(en)$_2$]Cl complex demonstrated a dose-dependent reduction in cell viability, with a concentration of 220 μg/mL proving to be the most effective, showing the highest level of cytotoxicity. The IC_{50} value was determined to be 100 ± 3.95 μg/mL, reflecting the concentration at which 50 % inhibition of cell viability occurred. In contrast, the MTT assay results for DL cells were less effective than those for U87 cells (Fig. 6C and D). Neither the ligand nor the [Co(intph)(en)$_2$]Cl exhibited a dose-dependent inhibition of DL cell viability. Additionally, the IC_{50} value for the [Co(intph)(en)$_2$]Cl complex against DL cells was found to be 120 μg/mL, which is higher than the IC_{50} observed in U87 cells. Consequently, further experiments were carried out on the U87 cell line. For these subsequent experiments, the [Co(intph)(en)$_2$]Cl complex was tested at three distinct doses: 60 μg/mL (low dose), 100 μg/mL (the previously determined IC_{50} concentration), and 140 μg/mL (higher dose).

3.7.2. [Co(intph)(en)$_2$]Cl treatment causes cell death by enhancing intracellular ROS production

We investigated the effects of [Co(intph)(en)$_2$]Cl treatment on U87 cells by employing Hoechst and PI double staining, observed through a fluorescent microscope. The integrity of the cytoplasmic membrane in dead cells, resulting from thiosemicarbazide treatment, allowed PI to penetrate U87 cells. Hoechst33342 binds to AT-rich region in the minor groove of DNA [50]. Cell classification was based on morphological and staining characteristics, early apoptotic cells displayed an intense blue fluorescence due to Hoechst33342 binding to condensed chromatin. Late apoptotic cells, allowing the entry of both PI and Hoechst33342, appeared as blue-violet fluorescence. In necrotic cells, PI penetrated due to a completely damaged cytoplasmic membrane, binding with fragmented DNA and emitting a bright red fluorescence (Fig. 7). This dual staining approach provided a comprehensive evaluation of U87 cell's responses, enabling the identification of early and late apoptotic cells, as well as necrotic cells [51]. Apoptosis mediated by mitochondria is predominantly triggered by an escalation in ROS generation within cells [52]. Consequently, we investigated the impact of [Co(intph)(en)$_2$]Cl treatment on ROS production in U87 cells. Through flow cytometry analysis of H_2DCFDA-stained cells, we observed a dose-dependent increase in ROS production, evidenced by the rightward shift of the histogram (Fig. 8 A). To further illustrate the magnitude of ROS generation, the higher fold change in the geometric mean, obtained through flow cytometry in relation to 2′, 7′-dichlorofluorescein's fluorescence, is depicted in a bar diagram (Fig. 8B). Additionally, cells stained with H_2DCFDA exhibited an enhanced intensity of green fluorescence when visualized under a confocal microscope, as compared to the control (Fig. 8C). These findings highlighted the dose-dependent elevation of ROS production in response to [Co(intph)(en)$_2$]Cl treatment. The observed elevation in ROS levels strongly suggests the occurrence of mitochondria-mediated apoptosis in U87 cells as a result of

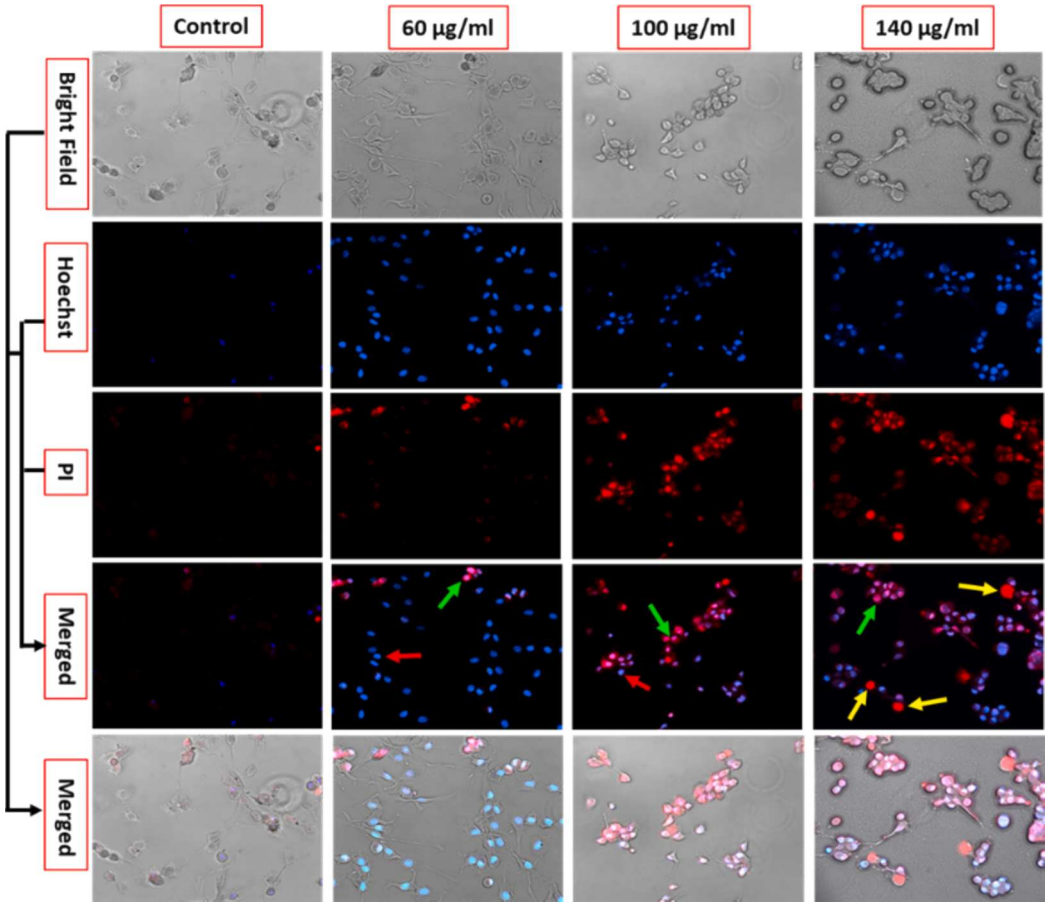

Fig. 7. Using HOECHST and PI staining, the changes in nuclear morphology and cell death caused by apoptosis and necrosis were evaluated. Early apoptotic cells were indicated by a red-colored arrow, indicating an intense bright blue fluorescence due to Hoechst staining of condensed chromatin. Late-apoptotic cells were marked with a green-colored arrow, exhibiting a blue-violet fluorescence, as both PI and Hoechst entered these cells. Finally, necrotic cells were denoted by a yellow-colored arrow, emitting bright red fluorescence exclusively due to PI staining, indicative of a completely damaged cytoplasmic membrane and fragmented DNA. Using Brightfield, DAPI, and TRITC channels, images were observed under fluorescent microscope (Nikon Eclipse 90i) at 20X magnification.

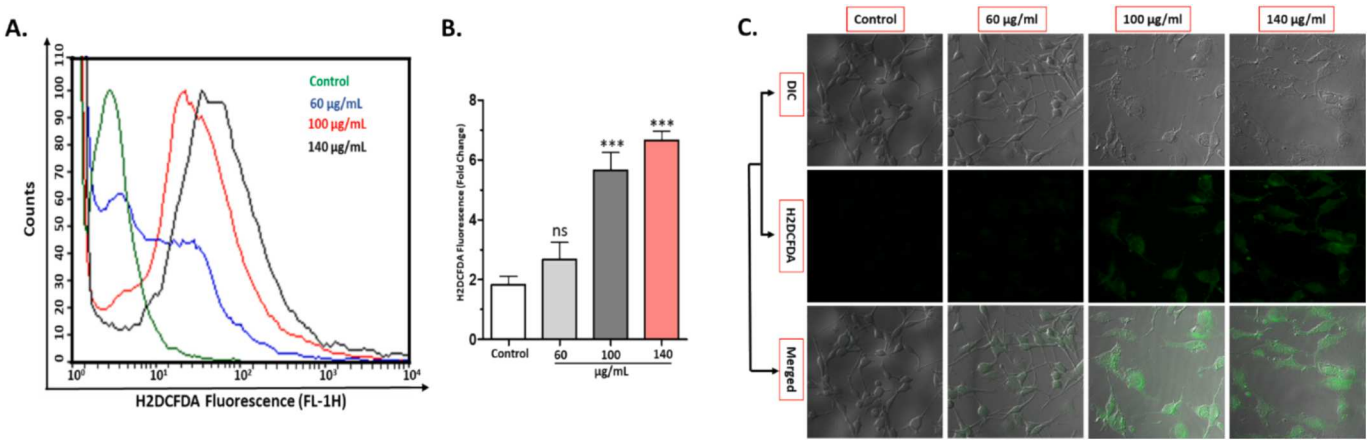

Fig. 8. The treatment effect of the Cobalt complex of thiosemicarbazide on ROS production by U87 cells was evaluated using H2DCFDA staining. ROS production was assessed by flow cytometry via the FL-1 channel and confocal microscopy (A) Shows enhanced ROS production, as indicated by the right shift in overlaid histograms. (B) Demonstrates an enhancement in the geo mean during flow cytometry. (C) Control and treated cells were visualized and photographed under confocal microscope (Zeiss LSM 780) by using of DIC, and FITC channels at 40× magnification.

thiosemicarbazide treatment. Our results bring out the promising anticancer activity of non-platinum metal complexes, specifically cobalt complexes of thiosemicarbazide, in combating glioblastoma, a highly malignant and aggressive form of brain cancer. Further exploration of the molecular mechanisms underlying this cytotoxicity may open the way for the development of effective anticancer strategies.

3.7.3. Comparative study of anticancer activity of complex [Co(intph)(en)$_2$]Cl with other reported compounds and standard drug

We evaluated the cytotoxic effects of the [Co(intph)(en)$_2$]Cl complex against the U87 glioblastoma cell line and compared its anticancer activity to that of previously reported compounds. There are relatively few studies addressing the antiproliferative effects of synthesized compounds on U87 cells. In our analysis, we compared the IC_{50} value of [Co(intph)(en)$_2$]Cl with those of other reported compounds and drugs under similar experimental conditions (Table 2). Our synthesized compound shows a lower IC_{50} value, indicating higher anticancer activity at a lower dose compared to Temozolomide, the standard treatment for glioblastoma multiforme, as well as several other compounds listed in Table 2. This suggests that [Co(intph)(en)$_2$]Cl demonstrates a significant improvement in efficacy against the human glioblastoma cells.

Table 2
Comparisons of IC_{50} value of [Co(intph)(en)$_2$]Cl with previously reported compounds against glioblastoma multiforme cells.

Compounds	IC_{50} values (µg/mL)	Ref.
Temozolomide (standard anticancer drug of Glioblastoma multiforme)	141.7	[53]
[Cu(L^2) (CH_3CN)$_2$](ClO_4)$_2$	93.5 (±6.3)	[54]
[Co(L_1)$_2$(Zn)$_2$(NO_3)$_3$(DMF)]	118 (±7.6)	[55]
[Co(L_2)$_3$Zn(NO_3)$_2$]	126 (±2.8)	[55]
[Co(L_2)$_3$Cd(NO3)$_2$]	61.6 (±1.4)	[55]
[Co(intph)(en)$_2$]Cl	100 ± 3.95	Present study

4. Conclusions

Here, we report the syntheses, characterization, and molecular structure of H_2*intph* and [Co((*intph*)(*en*)$_2$]Cl. The molecular structure of H_2*intph* and [Co((*intph*)(*en*)$_2$]Cl are stabilized by different weak intermolecular interactions viz. O-H···O, N-H···O, C-H···O, N-H···N, and C-H···Cl, leading to supramolecular architecture that has been further ascertained by Hirshfeld surface analysis. The fluorescence studies reveal among the ligand and its complex, the fluorescent behavior of the complex was found comparatively better than the free H_2*intph*. The geometry around Co(III) ion is distorted octahedral in complex. Further, *in vitro,* investigation established a significant tumoricidal effect of H_2*intph* and [Co((*intph*)(*en*)$_2$]Cl against U87 and DL cells. The Co(III) complex demonstrated significantly higher growth inhibition as compared to free ligand H_2*intph* against both U87 and DL cells. [Co((*intph*)(*en*)$_2$]Cl demonstrated impressive tumoricidal activity against human glioblastoma cells than the standard drugs (Temozolomide) of glioblastoma, and other earlier reported compounds. The increased levels of ROS strongly indicate that thiosemicarbazide Co(III) complex treatment induces mitochondria-mediated apoptosis in U87 cells. Our findings highlighted the potential anticancer effectiveness of non-platinum metal complexes, mainly cobalt thiosemicarbazide complex, in addressing glioblastoma, an extremely malignant and aggressive type of human brain cancer. In conclusion, delving deeper into the molecular mechanisms behind this cytotoxic effect could pave the way for the development of novel and potent anticancer strategies.

CRediT authorship contribution statement

Ram Nayan Gautam: Writing – review & editing, Writing – original draft, Visualization, Methodology, Investigation, Formal analysis, Data curation. **Alok Shukla:** Writing – original draft, Methodology, Formal analysis, Data curation. **Suryansh Chandra:** Software, Formal analysis, Data curation. **Sundeep Kumar:** Software, Formal analysis, Data curation. **A. Acharya:** Supervision, Formal analysis, Data curation, Conceptualization. **Mamata Singh:** Visualization, Software, Formal analysis, Data curation. **R.J. Butcher:** Validation, Software, Formal analysis, Data curation. **M.K. Bharty:** Writing – review & editing, Writing – original draft, Validation, Supervision, Resources, Project administration, Methodology, Investigation, Funding acquisition, Formal analysis, Conceptualization.

Declaration of competing interest

The authors declare that they have no known competing financial interests or personal relationships that could have appeared to influence the work reported in this paper.

Acknowledgments

Dr. M.K. Bharty expresses gratitude to BHU for the financial support provided through the IoE Research Grant for Faculty Development

Scheme No. 6031. Ram Nayan Gautam is also acknowledging the University Grant Commission (UGC), New Delhi for financial assistance in the form of a Senior Research Fellow, Ref No.: 139/(CSIR-UGC NET JUNE 2018).

Appendix A. Supplementary data

Supplementary crystallographic data for ligand and complex can be obtained through CCDC 2264277 and 2255821. Supplementary data to this article can be found online at https://doi.org/10.1016/j.inoche.2024.113521.

Data availability

The authors confirm that the data supporting the findings of this study are available within the article or in its Supplementary materials.

References

[1] M.-M. Inda, R. Bonavia, J. Seoane, Glioblastoma Multiforme: A Look Inside Its Heterogeneous Nature, Cancers (Basel) 6 (2014) 226–239, https://doi.org/10.3390/cancers6010226.
[2] N. Rabah, F.-E. Ait Mohand, N. Kravchenko-Balasha, Understanding Glioblastoma Signaling, Heterogeneity, Invasiveness, and Drug Delivery Barriers, Int. J. Mol. Sci. 24 (2023) 14256, https://doi.org/10.3390/ijms241814256.
[3] F. Torrisi, C. Alberghina, S. D'Aprile, A.M. Pavone, L. Longhitano, S. Giallongo, D. Tibullo, M. Di Rosa, A. Zappalà, F.P. Cammarata, G. Russo, M. Ippolito, G. Cuttone, G. Li Volti, N. Vicario, R. Parenti, The Hallmarks of Glioblastoma: Heterogeneity, Intercellular Crosstalk and Molecular Signature of Invasiveness and Progression, Biomedicines 10 (2022) 806, https://doi.org/10.3390/biomedicines10040806.
[4] F. Seker-Polat, N. Pinarbasi Degirmenci, I. Solaroglu, T. Bagci-Onder, Tumor Cell Infiltration into the Brain in Glioblastoma: From Mechanisms to Clinical Perspectives, Cancers (Basel) 14 (2022) 443, https://doi.org/10.3390/cancers14020443.
[5] E.K. Noch, R. Ramakrishna, R. Magge, Challenges in the Treatment of Glioblastoma: Multisystem Mechanisms of Therapeutic Resistance, World Neurosurg. 116 (2018) 505–517, https://doi.org/10.1016/j.wneu.2018.04.022.
[6] S.A. Aldossary, Review on Pharmacology of Cisplatin: Clinical Use, Toxicity and Mechanism of Resistance of Cisplatin, Biomed. Pharmacol. J. 12 (2019) 07–15, https://doi.org/10.13005/bpj/1608.
[7] A. Singh, K. Shiv, R. Singh, M.K. Bharty, P.P. Manna, L.B. Prasad, Antiproliferative activity of Fe (II), Co (II), Ni (II), Cu (II), and Zn(II) complexes of dithiocarbamate: synthesis, structural characterization, and thermal studies, Dalton Trans. 53 (2024) 1196–1208, https://doi.org/10.1039/D3DT03724J.
[8] K. Kar, D. Ghosh, B. Kabi, A. Chandra, A concise review on cobalt Schiff base complexes as anticancer agents, Polyhedron 222 (2022) 115890, https://doi.org/10.1016/j.poly.2022.115890.
[9] P.C. Bruijnincx, P.J. Sadler, New trends for metal complexes with anticancer activity, Curr. Opin. Chem. Biol. 12 (2008) 197–206, https://doi.org/10.1016/j.cbpa.2007.11.013.
[10] C.R. Munteanu, K. Suntharalingam, Advances in cobalt complexes as anticancer agents, Dalton Trans. 44 (2015) 13796–13808, https://doi.org/10.1039/C5DT02101D.
[11] S. Okamoto, L.D. Eltis, The biological occurrence and trafficking of cobalt, Metallomics 3 (2011) 963, https://doi.org/10.1039/c1mt00056j.
[12] M.A. Zoroddu, J. Aaseth, G. Crisponi, S. Medici, M. Peana, V.M. Nurchi, The essential metals for humans: a brief overview, J. Inorg. Biochem. 195 (2019) 120–129, https://doi.org/10.1016/j.jinorgbio.2019.03.013.
[13] K. Jomova, M. Makova, S.Y. Alomar, S.H. Alwasel, E. Nepovimova, K. Kuca, C. J. Rhodes, M. Valko, Essential metals in health and disease, Chem. Biol. Interact. 367 (2022) 110173, https://doi.org/10.1016/j.cbi.2022.110173.
[14] S.K. Kushawaha, R.K. Dani, M.K. Bharty, U.K. Chaudhari, V.K. Sharma, R. N. Kharwar, N.K. Singh, Studies on N-picolinoyl-N′-benzothioylhydrazide and its Zn(II) complex: Synthesis, structure, antibacterial activity, thermal analysis and DFT calculation, J. Mol. Struct. 1063 (2014) 60–69, https://doi.org/10.1016/j.molstruc.2014.01.043.
[15] R.P. John, A. Sreekanth, M.R. Prathapachandra Kurup, A. Usman, A.R. Ibrahim, H.-K. Fun, Spectral studies and structure of a 2-hydroxyacetophenone 3-hexamethyleneiminyl thiosemicarbazonate(-2) copper(II) complex containing 1,10-phenanthroline, Spectrochim. Acta A Mol. Biomol. Spectrosc. 59 (2003) 1349–1358, https://doi.org/10.1016/S1386-1425(02)00332-3.
[16] A. Siwek, J. Stefanska, Antimicrobial Activity and SAR Study of Some Novel Thiosemicarbazide Derivatives Bearing Piperidine Moiety, Med. Chem. (Los Angeles) 7 (2011) 690–696, https://doi.org/10.2174/157340611797928406.
[17] B. Holló, M.V. Rodić, L.S. Vojinović-Ješić, V. Živković-Radovanović, G. Vučković, V.M. Leovac, K.M. Szécsényi, Crystal structure, thermal behavior, and microbiological activity of a thiosemicarbazide-type ligand and its cobalt complexes, J. Therm. Anal. Calorim. 116 (2014) 655–662, https://doi.org/10.1007/s10973-013-3489-1.
[18] H.A. El-Ghamry, A. Fawzy, T.A. Farghaly, T.M. Bawazeer, N. Alqarni, F. M. Alkhatib, M. Gaber, Evaluation of the efficiency of divalent cobalt and copper chelates based on isatin derivatives and thiosemicarbazide ligands as inhibitors for the corrosion of Sabic iron in acidic medium, Arab. J. Chem. 15 (2022) 103522, https://doi.org/10.1016/j.arabjc.2021.103522.
[19] N.N.M. Ishak, J. Jamsari, A.Z. Ismail, M.I.M. Tahir, E.R.T. Tiekink, A. Veerakumarasivam, T.B.S.A. Ravoof, Synthesis, characterisation and biological studies of mixed-ligand nickel (II) complexes containing imidazole derivatives and thiosemicarbazide Schiff bases, J. Mol. Struct. 1198 (2019) 126888, https://doi.org/10.1016/j.molstruc.2019.126888.
[20] T.A. Yousef, G.M. Abu El-Reash, O.A. El-Gammal, S.F. Ahmed, Structural, DFT and biological studies on Cu(II) complexes of semi and thiosemicarbazide ligands derived from diketo hydrazide, Polyhedron 81 (2014) 749–763, https://doi.org/10.1016/j.poly.2014.07.035.
[21] A.M. Thomas, A.D. Naik, M. Nethaji, A.R. Chakravarty, Synthesis, crystal structure and photo-induced DNA cleavage activity of ternary copper(II)-thiosemicarbazone complexes having heterocyclic bases, Inorganica Chim Acta 357 (2004) 2315–2323, https://doi.org/10.1016/j.ica.2004.01.031.
[22] H.S. Seleem, B.A. El-Shetary, S.M.E. Khalil, M. Mostafa, M. Shebl, Structural diversity in copper(II) complexes of bis(thiosemicarbazone) and bis (semicarbazone) ligands, J. Coord. Chem. 58 (2005) 479–493, https://doi.org/10.1080/00958970512331334269.
[23] S. Caglar, A. Altay, M. Kuzucu, B. Caglar, In Vitro Anticancer Activity of Novel Co (II) and Ni(II) Complexes of Non-steroidal Anti-inflammatory Drug Niflumic Acid Against Human Breast Adenocarcinoma MCF-7 Cells, Cell Biochem. Biophys. 79 (2021) 729–746, https://doi.org/10.1007/s12013-021-00984-z.
[24] M.N. Patel, P.A. Dosi, B.S. Bhatt, Square planar palladium(II) complexes of bipyridines: synthesis, characterization, and biological studies, J. Coord. Chem. 65 (2012) 3833–3844, https://doi.org/10.1080/00958972.2012.727207.
[25] M.K. Gond, S.K. Pandey, R. Singh, M.K. Bharty, P.P. Manna, V.K. Singh, B. Maiti, L. B. Prasad, R.J. Butcher, *In vitro* and *In silico* anticancer activities of Mn(II), Co(II), and Ni(II) complexes: synthesis, characterization, crystal structures, and DFT studies, New J. Chem. 46 (2022) 11056–11070, https://doi.org/10.1039/D2NJ00264G.
[26] U. Brahma, R. Kothari, P. Sharma, V. Bhandari, Antimicrobial and anti-biofilm activity of hexadentated macrocyclic complex of copper (II) derived from thiosemicarbazide against Staphylococcus aureus, Sci. Rep. 8 (2018) 8050, https://doi.org/10.1038/s41598-018-26483-5.
[27] A. Singh, M.K. Bharty, R.K. Dani, S. Singh, S.K. Kushawaha, N.K. Singh, Manganese (II) and zinc(II) complexes of 4-phenyl(2-methoxybenzoyl)-3-thiosemicarbazide: Synthesis, spectral, structural characterization, thermal behavior and DFT study, Polyhedron 73 (2014) 98–109, https://doi.org/10.1016/j.poly.2014.02.029.
[28] N. Biswas, S. Khanra, A. Sarkar, S. Bhattacharjee, D. Prasad Mandal, A. Chaudhuri, S. Chakraborty, C. Roy Choudhury, One new azido bridged dinuclear copper(II) thiosemicarbazide complex: synthesis, DNA/protein binding, molecular docking study and cytotoxicity activity, New J. Chem. 41 (2017) 12996–13011, https://doi.org/10.1039/C7NJ01998J.
[29] Y. Zhang, Y.X. Su, Z. Cai, L. Tong, W.K. Dong, Structural, fluorescent and theoretical studies of a more flexible salamo-type ligand and its uncommon tetranuclear chloride-bridged nickel (II) complex, J. Mol. Struct. 1309 (2024), https://doi.org/10.1016/j.molstruc.2024.138164, 138164.
[30] L.L. Gan, H.Y. Niu, L.L. Liu, W.K. Dong, Y.J. Ding, The effect of different counter-anions on two nonsymmetric salamo-type copper (II) complexes with different structures, J. Mol. Struct. 1302 (2024) 137526.
[31] L. Tong, Y.F. Ding, X. Li, L.L. Man, W.K. Dong, Synthesis, crystal structure, fluorescence properties, and theoretical studies of a dinuclear Ni (II) complex derived from a quinoline-containing half-salamo-type ligand, J. Coord. Chem. 76 (2023) 1635–1649, https://doi.org/10.1080/00958972.2023.2263619.
[32] Y. Zhang, Y.B. Yan, R.W. Yang, R. Chen, W.K. Dong, Exploring the structure, fluorescence properties and theoretical studies of newly synthesized Co (II), Ni (II) and Cd (II) complexes bearing acylhydrazone ligands, J. Mol. Struct. 1314 (2024), https://doi.org/10.1016/j.molstruc.2024.138840, 138840.
[33] M.K. Bharty, R.K. Dani, N.K. Singh, R.J. Butcher, Polymeric, dimeric and monomeric Mn(II) complexes derived from [N′-(pyridine-4-carbonyl)-hydrazine]-carbodithioic acid methyl ester and 1-isonicotinoyl-4-phenyl-3-thiosemicarbazide: Syntheses, crystal structure and thermal analysis, Polyhedron 112 (2016) 67–77, https://doi.org/10.1016/j.poly.2016.03.050.
[34] A. Singh, L.B. Prasad, K. Shiv, R. Kumar, S. Garai, Synthesis, characterization, and in vitro antibacterial and cytotoxic study of Co(II), Ni(II), Cu(II), and Zn(II) complexes of N-(4-methoxybenzyl) N-(phenylethyl) dithiocarbamate ligand, J. Mol. Struct. 1288 (2023), https://doi.org/10.1016/j.molstruc.2023.135835, 135835.
[35] F.H. Allen, O. Kennard, D.G. Watson, L. Brammer, A.G. Orpen, R. Taylor, Tables of bond lengths determined by X-ray and neutron diffraction. Part 1. Bond lengths in organic compounds, J. Chem. Soc., Perkin Trans. 2 (1987) S1, https://doi.org/10.1039/p298700000s1.
[36] S.K. Pandey, S. Gupta, S. Jaiswal, M.K. Gond, M.K. Bharty, R.J. Butcher, Synthesis, Characterizations, Crystal Structure, DFT, and Hirshfeld Surface Analysis of 4-Cyclohexyl-1-(thiophene-2-carbonyl)thiosemicarbazide, J. Chem. Crystallogr. 53 (2023) 244–255, https://doi.org/10.1007/s10870-022-00965-x.
[37] M. Wos, M. Miazga-Karska, A.A. Kaczor, K. Klimek, Z. Karczmarzyk, D. Kowalczuk, W. Wysocki, G. Ginalska, Z. Urbanczyk-Lipkowska, M. Morawiak, M. Pitucha, Novel thiosemicarbazide derivatives with 4-nitrophenyl group as multi-target drugs: α-glucosidase inhibitors with antibacterial and antiproliferative activity, Biomed. Pharmacother. 93 (2017) 1269–1276, https://doi.org/10.1016/j.biopha.2017.07.049.

[38] P. Gautam, O. Prakash, R.K. Dani, M.K. Bharty, N.K. Singh, R.K. Singh, Spectra-structure correlation based study of complex molecules of 1-isonicotinoyl-3-thio-semicarbazide with Ni^{2+}, Mn^{2+} and Fe^{3+} using Raman, UV–visible and DFT techniques, J. Mol. Struct. 1127 (2017) 489–497, https://doi.org/10.1016/j.molstruc.2016.07.095.

[39] R.K. Dani, M.K. Bharty, O. Prakash, R.K. Singh, B. Prashanth, S. Singh, N.K. Singh, Ni(II) and Co(III) complexes of 5-methyl-1,3,4-thiadiazole-2-thiol: syntheses, spectral, structural, thermal analysis, and DFT calculation, J. Coord. Chem. 68 (2015) 2666–2681, https://doi.org/10.1080/00958972.2015.1057131.

[40] S. Chandra, S. Jaiswal, A. Shukla, A.K. Singh, S. Garai, A. Bharti, A. Acharya, M. K. Bharty, Solvent-dependent crystallization and anti-cancer activities based on Ni (II) and Co(II) complexes of 1-picolinoyl-4-phenyl-3-thiosemicarbazide: Synthesis, crystal structure, and photoluminescence study, J. Mol. Struct. 1294 (2023) 136473, https://doi.org/10.1016/j.molstruc.2023.136473.

[41] A. Singh, R. Kumar, R. Patel, R.N. Gautam, M.K. Bharty, L.B. Prasad, Dithiocarbamate-based novel anti-histaminic agents: synthesis, characterization, crystal structure and thermal study, Dalton Trans. 53 (2024) 14077–14088, https://doi.org/10.1039/D4DT01777C.

[42] P.K. Maniyampara, L.K. Suresh, K. Jayakumar, E. Manoj, M.P. Kurup, Novel cobalt complexes of pyridine-based NNS donor thiosemicarbazones: Synthesis, X-ray characterization, DFT calculations, Hirshfeld surface analysis, and molecular docking study, J. Mol. Struct. 1275 (2023), https://doi.org/10.1016/j.molstruc.2022.134680, 134680.

[43] M.K. Bharty, A.K. Srivastava, R. Dulare, R.J. Butcher, N.K. Singh, Synthesis, spectral and X-ray structural studies of Ni(II) complexes of N′-acylhydrazine carbodithioic acid esters containing ethylenediamine or o-phenanthroline as coligands, Polyhedron 30 (2011) 990–996, https://doi.org/10.1016/j.poly.2010.12.043.

[44] S. Paswan, M.K. Bharty, U.K. Chaudhari, R. Chaurasia, R.J. Butcher, J.P. Jasinski, Syntheses, spectral and structural characterization of Cd(II) complexes of 5-(thiophen-2-yl)-1,3,4-oxadiazole-2-thione, 2-thiohydantoin and 2-thenoyltrifluoroacetone, Polyhedron 133 (2017) 137–145, https://doi.org/10.1016/j.poly.2017.05.012.

[45] V. Suni, M.P. Kurup, M. Nethaji, Studies on Co (II) and Co (III) complexes of di-2-pyridyl ketone N (4)-cyclohexyl and N (4)-phenyl thiosemicarbazones, Polyhedron 26 (2007) 5203–5209, https://doi.org/10.1016/j.poly.2007.07.051.

[46] R. Dulare, M.K. Bharty, A. Singh, N.K. Singh, Synthesis, spectral and structural studies of 1-ethoxycarbonyl-piperazine-4-carbodithioate and its Co(III), Zn(II) and Cd(II) complexes, Polyhedron 31 (2012) 373–378, https://doi.org/10.1016/j.poly.2011.09.036.

[47] S. Jaiswal, S.K. Pandey, J. Prajapati, S. Chandra, M.K. Gond, M.K. Bharty, I. Tiwari, R.J. Butcher, Cd(II) complexes derived from thiazoline, hydrazide and carbodithioate ligands: synthesis, crystal structures and electrochemical sensing of uric acid, Appl. Organomet. Chem. 37 (2023), https://doi.org/10.1002/aoc.7085.

[48] D. Majumdar, S. Roy, A. Frontera, R.M. Gomila, T.K. Pal, Crystal engineering of Pb (II)-salen coordination polymer enforced for the selective fluorescence NACs sensing activity in a dispersed aqueous medium: A combined experimental and theoretical DFT monologue, J. Mol. Struct. 1276 (2023) 134717, https://doi.org/10.1016/j.molstruc.2022.134717.

[49] S. Chandra, J. Prajapati, S. Jaiswal, S.K. Pandey, I. Tiwari, L.B. Prasad, M. K. Bharty, Electrochemical sensing of 4-nitrophenol through heteroleptic complexes of Ag(I) and Hg(II) based on 2-thiazoline-2-thiol: Synthesis, crystal structures, and Hirshfeld analysis, Appl. Organomet. Chem. 37 (2023), https://doi.org/10.1002/aoc.7210.

[50] G.S. Batibay, G. Keser Karaoglan, G. Gumrukcu Kose, E. Ozcelik Kazancioglu, E. Metin, F. Danisman Kalindemirtas, S. Erdem Kuruca, N. Arsu, DNA groove binder and significant cytotoxic activity on human colon cancer cells: Potential of a dimeric zinc (II) phthalocyanine derivative, Biophys. Chem. 295 (2023) 106974, https://doi.org/10.1016/j.bpc.2023.106974.

[51] A. Rogalska, A. Gajek, M. Szwed, Z. Jóźwiak, A. Marczak, The role of reactive oxygen species in WP 631-induced death of human ovarian cancer cells: A comparison with the effect of doxorubicin, Toxicol. In Vitro 25 (2011) 1712–1720, https://doi.org/10.1016/j.tiv.2011.08.009.

[52] H. El-Osta, M.L. Circu, Mitochondrial ROS and Apoptosis, in: Mitochondrial Mechanisms of Degeneration and Repair in Parkinson's Disease, Springer International Publishing, Cham, 2016: pp. 1–23. https://doi.org/10.1007/978-3-319-42139-1_1.

[53] A.R. Afshari, M. Karimi Roshan, M. Soukhtanloo, A. Ghorbani, F. Rahmani, M. Jalili-Nik, M.M. Vahedi, A. Hoseini, H.R. Sadeghnia, H. Mollazadeh, S. H. Mousavi, Cytotoxic effects of auraptene against a human malignant glioblastoma cell line, Avicenna J. Phytomed. 9 (2019) 334–346.

[54] A.P. Singh, N.K. Kaushik, A.K. Verma, G. Hundal, R. Gupta, Synthesis, structure and biological activity of copper(II) complexes of 4-(2-pyridylmethyl)-1,7-dimethyl-1,4,7-triazonane-2,6-dione and 4-(2-pyridylethyl)-1,7-dimethyl-1,4,7-triazonane-2,6-dione, Eur. J. Med. Chem. 44 (2009) 1607–1614, https://doi.org/10.1016/j.ejmech.2008.07.029.

[55] N.K. Kaushik, A. Mishra, A. Ali, J.S. Adhikari, A.K. Verma, R. Gupta, Synthesis, characterization, and antibacterial and anticancer screening of M2+–Co3+–M2+ and Co3+–M2+ (M is Zn, Cd, Hg) heterometallic complexes, J. Biol. Inorg. Chem. 17 (2012) 1217–1230, https://doi.org/10.1007/s00775-012-0937-5.